Time-domain Modelling of Grid-connected CHP for its Interaction with the Power Grid

Da Xie, *Member, IEEE*, Aikang Chen, Chenghong Gu, *Member, IEEE*, Jun Tai

***Abstract*—This paper presents a nonlinear dynamic model of grid-connected combined heat and power system (CHP) that can effectively simulate the thermoelectric interaction and examine the impact of the CHP on the power grid. Based on the theorems of mass balance and energy balance, this paper studies and analyses the principles and dynamic characteristics of the main CHP components, including gas internal combustion engine, synchronous generator, waste heat exchanger, water storage tank, exhaust-heat boiler, and gas fired boiler. Then, the nonlinear time domain models for each component are built against input and output parameters in order to facilitate the study of CHP operation under various conditions. Subsequently, a simulation method that can deal with the coupling of all models with different time constants is proposed. Finally, dynamic simulation analysis of the developed CHP model is carried out on the MATLAB/Simulink. Extensive demonstration results show that the developed models are accurate to represent the thermoelectric interactions in the gird-connected CHP and capture the impact of this gird-connected CHPs on the power grid. This study is particularly beneficial to the design of new control strategies for CHPs to maximise its efficiency and stability value to the grid.**

***Index Terms*—Grid-connected combined heat and power system, time domain model, dynamic simulation, interaction.**

I. Introduction

COMBINED heat and power system (CHP), which has high energy utilization and low emission, is a feasible technology in regulating thermal and electrical load flexibly [1]. CHP can produce heat and electricity through a single process by using oil or natural gas with the efficiency more than 80%, which overwhelms the average thermal efficiency of traditional generation (30%~35%) [2]. Besides, CHP is increasingly used by industrial and residential customers because of its ability to adjust the output ratio of heat and electricity [3]. Analyses of principle and dynamic characteristics of CHP are of great significance to understand the performance under various system loading conditions and the resilience to external disturbances that underlie optimization and control.

Current studies mainly represent CHP by static models and focus on investigating its optimal operation for maximizing economic and environmental benefits. A nonlinear model is developed in [4] for optimal operation and economic benefits of combined heating, cooling and power systems. The authors of [5] establish the profit optimization model of grid-connected CHP based on the operation curve and forecasted real-time energy prices from energy market. A series of environmental impact models are constructed in [6] to compare the loss differences between traditional cold/heat separate generation and CHP. A multi-objective optimization model for CHP in real conditions is set up in [7], which considers the impact of technologies, economic, energy, and environment. The authors of [8] present a comprehensive CHP model, which contains different heat and power units, to study the imbalances in two-price balancing market.

However, few researchers address the dynamic model of a grid-connected CHP. Authors of [9] explore the key parameters that impact on a university campus CHP performance with its dynamic model, but the model of the boiler is established as a lumped model. In [10], mathematical models of cogeneration steam turbines are developed for a full-scale investigation into energy efficiency improvement of CHPs, but the modelling process is not detailed. And the dynamic model of a direct-combustion biomass CHP is constructed in [11] to provide a reliable platform for control strategy research, but the system that consists of a biomass combustion, a boiler-turbine, and a district heating network model is too simple to represent most systems. In addition, these models all neglect the grid-connected scenario. Spurred by the government policy, the urban multi-energy network is increasingly interconnected with the rise in penetration of CHPs [12]. The development of interaction with the power grid is important for studying the stability and dispatch of the system, and the first step is constructing the grid-connected CHP model.

At present, the research on the dynamic modelling of the CHP is at an early stage. The authors of [13] develop a full MATLAB model, which contains internal combustion engine with generator, electrical storage, and thermal storage. However, there are no detailed formulas for modelling. A simplified dynamic model of micro-CHP is developed in [14]. The output variables of the model are compared with the operating data collected in reality to verify model accuracy. A

This work was supported in part by the Shanghai Committee of Science and Technology under Grant 16DZ1202800 and the Engineering and Physical Sciences Research Council under Grant EP/M000141/1.

D. XIE and A. CHEN are with the department of Electronic Information and Electrical Engineering, Shanghai Jiao Tong University, Shanghai, 200240, China (e-mail: xieda@sjtu.edu.cn; 381315687@sjtu.edu.cn).

C. GU is with the department of Electronic and Electrical Engineering, University of Bath, Bath, BA2 7AY, UK (e-mail: C.Gu@bath.ac.uk).

J. TAI is with the Shanghai Environmental Sanitation Engineering Design Institute, Shanghai, 200232, China (e-mail: taijun8011@163.com).

detailed and joint CHP dispatch model based on the principle of three-stage heat transfer is proposed in [15]. Referred to Rowen model, [16] proposes an implemented model of CHP, which focuses on the prime mover dynamics. To summarize, the CHP models in [14], [15] and [16] are incomprehensive, where many components are not considered.

CHPs are playing an essential role in our current energy mix because of its high efficiency and low emissions. However, there are still many challenges in effectively and efficiently control CHPs in response to the various electricity and heating demand, which is largely due to the lack of representative CHP models. The developed models in this paper bridge the research gap from the following aspects:

- The model contains gas internal combustion engine, synchronous generator, waste heat exchanger, water storage tank, exhaust-heat boiler and gas fired boiler. Compared with existing models, the model developed is more detailed and more systematic, so that the internal changes induced by different controls can be comprehensively reflected in an explicit way.
- The model contains a group of component models connected by their inputs and outputs. Hence, the relationships between the input and output of all components are captured by the CHP model, facilitating control strategy design that underline the robust regulation of each equipment.
- The power grid and heat network are considered in the CHP modelling. Thus, the analysis of the grid-connected CHPs can be performed to underlie the control methods for CHPs with the consideration of their impact on the systems.

The contributions of this paper are threefold: i) it establishes the nonlinear time-domain model based on MATLAB for a grid-connected CHP, which underlines further research on optimal control design and dynamic analysis; ii) it investigates the dynamic characteristics of main components in a grid-connected CHP under small disturbances. Thus, the key parameters that affect dynamic performance are captured; iii) the impact of a grid-connected CHP on the grid is extensively studied. Demonstration results illustrate the contribution to the stability of the multi-energy system from CHPs.

The remainder of this paper is organized as follows. In Section II, based on the working principle and dynamic characteristics of each component of the grid-connected CHP, nonlinear dynamic models are built respectively. Section III discusses the problem of different time constants in the system model and proposes a mitigation method. Dynamic simulation analysis is performed on the MATLAB/Simulink platform in Section IV. Section V concludes the paper.

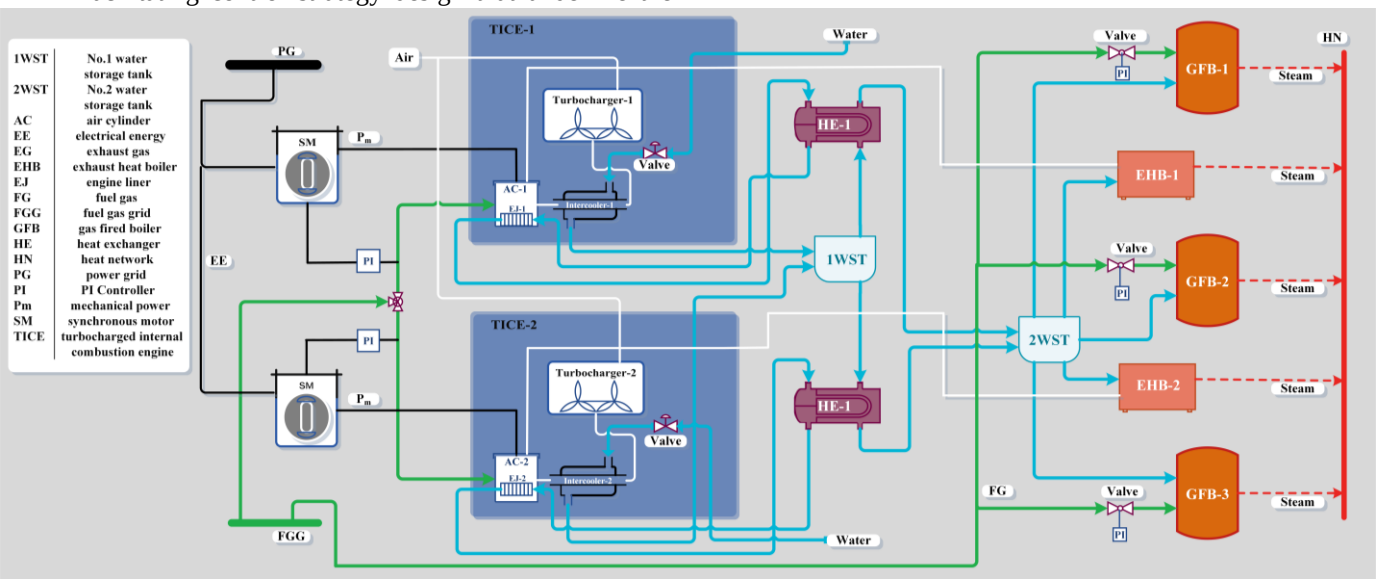

Fig. 1. Structure diagram of grid-connected combined heat and power system

II. Dynamic Modelling Of CHP

The structure of the CHP, which is composed of gas internal combustion engine, synchronous generator, exhaust heat exchanger, water storage tank, exhaust heat boiler and gas-fired boiler, is structurally diagrammed in Fig. 1.

A. Modelling of gas internal combustion engine

The model of the gas internal combustion engine is divided into six parts, compressor, turbine, turbocharger, intercooler, air cylinder, and controller. The focus in the modelling is the input and output parameters of each element. Furthermore, in order to simplify the model, the internal specific thermodynamic processes are ignored and the method of mean value modelling is utilized [17]. Mean value model is built on the quasi-steady model, which describes the representative change process using the simplest first-order differential equations. It is an empirical formula to express the complex physical model, mainly focusing on the average of each variable that changes over time [18].

In order to facilitate the modelling, the following simplification is introduced [19]: (1) The influences of air pressure and other factors on the performance of internal combustion engine are ignored. (2) The volume inertia and energy lag of each component are not considered. (3) The motion of the fluid in the internal combustion engine is

assumed to be one-dimensional and the fusion of gas in the gas cylinder is completed in an instant, with uniform gas distribution. (4) Thermal decomposition and heat loss during combustion are neglected. (5) The working fluid in the internal combustion engine is in the ideal state, and its specific heat, specific enthalpy, and specific internal energy can only be affected by its temperature and composition.

The structural diagram of each part of the gas internal combustion engine is shown in Fig. 2.

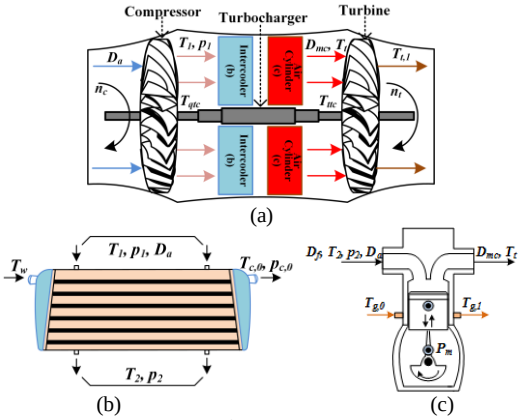

Fig. 2. Structural model diagram of gas engine. (a) Turbine compressor. (b) Intercooler. (c) Air cylinder.

1) Compressor

The input parameters of the compressor are rotational speed of the compressor n_c and air intake flow D_a, and the output parameters of the compressor are outlet air temperature T_1 and the torque consumed by the compressor T_{qtc}. Hence, the following empirical formulas can be derived from thermal energy balance and torque equilibrium [19]:

$$T_1 = T_0\left[1+(1/\eta_c)\left(\pi_c^{(k-1)/k}-1\right)\right] \tag{1}$$

$$T_{\mathrm{qtc}} = \frac{1}{\eta_c}\frac{k}{k-1}\frac{30D_aRT_0(\pi_c^{(k-1)/k}-1)}{\pi_c n_c} \tag{2}$$

Where T_0 is the temperature of the air, k represents the air adiabatic index, π_c and η_c are the pressure ratio and efficiency of the compressor, and R represents the gas constant.

2) Turbocharger

The input parameters of the turbocharger are the torque consumed by compressor T_{qtc} and the output torque of the turbine T_{ttc}, and the output parameters of the turbocharger are rotational speed of turbine n_c which is equal to the rotational speed of the compressor in stable operation. According to the principles of rigid body dynamics of the axis of rotation, the equation between them can be obtained as follows:

$$I_{tc}\frac{\pi}{30}\frac{dn_c}{dt} = \eta_{tc}T_{ttc} - T_{qtc} \tag{3}$$

Where I_{tc} and η_{tc} are the moments of inertia of the rotating part and the mechanical efficiency of the turbocharger.

3) Turbine

The input parameters of the turbine are inlet exhaust gas temperature of turbine T_t, the rotational speed of turbine n_t and gas intake flow of the turbine D_{mc}, and the output parameters of the turbine are outlet exhaust gas temperature of turbine $T_{t,1}$ and output torque of turbine T_{ttc}. Similarly, the following empirical formulas can be derived from the energy balance and torque equilibrium [19]:

$$T_{t,1} = T_t\left\{1-\eta_t\left[1-(1/\pi_t)^{(k-1)/k}\right]\right\} \tag{4}$$

$$T_{ttc} = \eta_t\frac{k}{k-1}\frac{30D_{mc}RT_t\left[1-(1-\pi_t)^{(k-1)/k}\right]}{\pi_t n_t} \tag{5}$$

Where η_t and π_t are the efficiency and expansion ratio of the turbine.

4) Intercooler

In the model of the intercooler, algebraic equations are used to replace the differential equations on the premise where we ignore the effect of the temperature of heat exchange wall.

The compressor outlet air temperature T_1 and outlet flow D_a are the input parameters of the intercooler, and the output parameters are inlet water flow $D_{c,0}$ and inlet water temperature $T_{c,0}$ of No.1 water storage tank, and outlet air temperature T_2 of the intercooler. The following equations can be obtained from the energy conservation and the experience formula of heat/flow change in heat transfer process [19]:

$$T_2 = T_1(1-\phi_1)+\phi_1 T_w \tag{6}$$

$$T_{c,0} = K_1T_w + K_2T_1 \tag{7}$$

$$D_{c,0} = K_3D_a \tag{8}$$

Where ϕ_1 is the cooling efficiency, T_w is the cooling water temperature, and K_1, K_2, and K_3 represent the heat transfer coefficients and the flow ratio.

5) Gas cylinder

When the gas cylinder is constructed, the ratio of air and gas enter the gas cylinder is fixed, i.e., the air combustion ratio is a constant of 32. At the same time, considering that jacket water circulates in a closed space, its flow does not change, unlike its temperature. Therefore, jacket water flow is set as a constant, i.e., D_{mg}=3.99 kg/s.

The input parameters of the gas cylinder are outlet air temperature T_2 and pressure p_2 of the intercooler, inlet jacket water temperature $T_{g,0}$, gas flow D_f and air flow D_a entered in the air cylinder. The output parameters are exhaust gas flow D_{mc}, the temperature of exhaust gas T_t, mechanical power of the synchronous generator P_m, and outlet jacket water temperature $T_{g,1}$. The following formulas can be derived from thermal energy conservation and flow conservation:

$$D_{mc} = D_a + D_f \tag{9}$$

$$T_{g,1} = \varsigma_w D_f H_u/(C_w\cdot D_{mg}) + T_{g,0} \tag{10}$$

$$D_fH_u + D_aC_{pa}T_2 = P_m + (D_f+D_a)C_{pg}T_t + \varsigma_w D_f H_u \tag{11}$$

$$P_{\mathrm{m}} = \eta_m D_f H_u \tag{12}$$

Where C_w is the specific heat of jacket water, H_u is low heat value of gas, C_{pa} represents specific heat of inlet gas at constant pressure, C_{pg} represents specific heat of outlet gas at constant pressure, η_m is the generating efficiency, and ς_w is the heat absorbing efficiency.

6) Controller

The model of controller, which uses the proportional integral controller as the core, can regulate gas intake of the internal combustion engine D_f according to the difference between the expected P_{ex} and current active power P. It adjusts the

mechanical power P_m to control the output active power of the synchronous generator. Fig. 3 shows the flowchart of the controller.

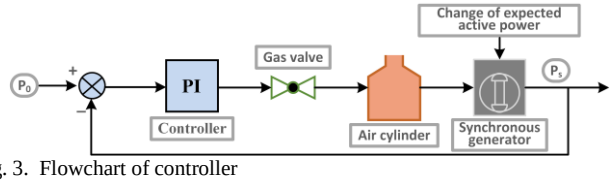

Fig. 3. Flowchart of controller

Fig. 4 clearly shows the structure of the exhaust heat exchanger. The following two hypotheses are made considering actual situations: (1) the model employs the average fluid temperature instead of the actual temperature for the process of heat exchange. (2) The changes of fluid flow and heat transfer coefficient are ignored in the model.

B. *Modelling of exhaust heat exchanger*

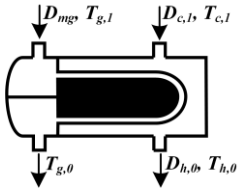

Fig. 4. Structural model diagram of exhaust heat exchange

The input parameters of the exhaust heat exchanger are outlet jacket water flow D_{mg} and temperature $T_{g,1}$, outlet water flow $D_{c,1}$ and temperature $T_{c,1}$ of the No. 1 water storage tank. The output parameters are inlet jacket water temperature $T_{g,0}$, inlet water flow $D_{h,0}$ and temperature $T_{h,0}$ of the No. 2 water storage tank. The relation formulas can be derived based on the thermodynamic theorem as follows [20]:

$$D_{mg}C_{p1}\left(T_{g,1}-T_{g,0}\right)=K_{e1}A_1\left(\left(T_{g,0}+T_{g,1}\right)/2-T_{hp}\right) \tag{13}$$

$$D_{c,1}C_{p2}\left(T_{h,0}-T_{c,1}\right)=K_{e2}A_2\left(T_{hp}-\left(T_{h,0}+T_{c,1}\right)/2\right) \tag{14}$$

$$mC_h\frac{dT_{hp}}{dt}=K_{e1}A_1\left(\frac{T_{g,0}+T_{g,1}}{2}-T_{hp}\right)-K_{e2}A_2\left(T_{hp}-\frac{T_{h,0}+T_{c,1}}{2}\right) \tag{15}$$

$$D_{h,0}=D_{c,1} \tag{16}$$

Where C_{p1} and C_{p2} are specific heat of water in exchanger, K_{e1} and K_{e2} are heat transfer coefficients of water, A_1 and A_2 are heat exchange surface of the pipe side and shell side, T_{hp} represents the average temperature and m is the mass of the exchange wall, and C_h is the specific heat of the exchange wall.

Considering the fixed capacity of water tank and jacket, this paper assumes the outlet water flow of jacket and No. 1 water tank are constant, respectively, D_{mg}=1.76 kg/s and $D_{c,1}$=2 kg/s.

C. *Modelling of water storage tank*

The CHP in this paper contains two water tanks, where the water of No.1 water tank comes from the intercooler of the gas internal combustion engine and goes to exhaust heat exchanger. The cooling water of the exhaust heat exchanger is the inflow water of No.2 tank, and then the outlet water is the fluid of the exhaust heat boiler and gas fired boiler.

The energy transfer of the water tank can concisely boil down to energy delivered to output water and dissipated in the environment. The model in this paper is built on the ensuing conditions: (1) The influence of the water level, the atmosphere of water tank, and water temperature on the water flow is neglected. (2) Equipment damage is not considered. (3) Outlet water flow only depends on the demand of boiler. The structure of the tank is shown in Fig. 5.

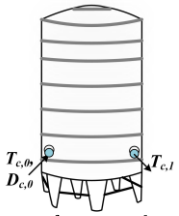

Fig. 5. Structural model diagram of water tank

In the model of No.1 water tank, outlet water flow can be set as constant by analysing actual data, namely, $D_{c,1}$=2 kg/s. Besides, the water in the tank defaults to the lowest capacity. Therefore, (17) can be obtained with the law of thermodynamics and empirical formulas for heat dissipation [21]. The input parameters of the water tank are inlet water flow $D_{c,0}$ and temperature $T_{c,0}$ of the No. 1 water storage tank. The output parameter is outlet water temperature $T_{c,1}$ of the No. 1 water storage tank.

$$\left[\left(\int\left(D_{c,0}-D_{c,1}\right)dt+M_0\right)\frac{dT_{c,1}}{dt}\right]=D_{c,0}T_{c,0}-D_{c,1}T_{c,1}-Q_{c,h}/C_w \tag{17}$$

Where C_w is the specific heat of water, M_0 is the mass of the lowest water, $Q_{c,h}$ represents the heat loss of No.1 water tank, $Q_{c,1}$ is the heat loss of insulation.

The model of No. 2 water tank is like the No.1, where it is assumed that the fluid flow of the boiler is fixed, i.e., $D_{yr,0}$=0.28 kg/s, and $D_{rq,0}$=1.1 kg/s.

When the inlet water flow is less than the outlet water flow, the water in tank will eventually drop to the level of the lowest water under regular operation. The energy equation of water tank needs to consider the energy of the external water supply. Here, this model assumes the addition of external water is right to maintain the balance of input and output water of the tank. Therefore, (17) is adjusted to (18).

$$M_0\frac{dT_{c,1}}{dt}=D_{c,0}T_{c,0}+D_{out}T_{out}-D_{c,1}T_{c,1}-\frac{Q_{c,h}}{C_w} \tag{18}$$

Where D_{out} and T_{out} represent the flow and temperature of external water.

D. *Modelling of exhaust heat boiler*

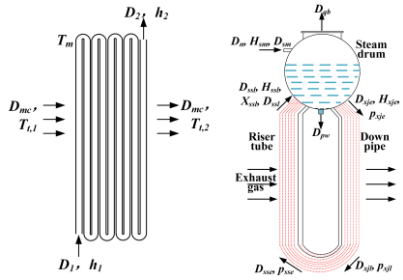

Fig. 6. Structural model diagram of exhaust heat exchange. (a) Single-phase region. (b) two-phase region.

In this paper, the model is divided into two parts: single-phase region and two-phase region, whose structural models are shown in Fig. 6.

1) Single-phase region

The single-phase region means that the fluid in the pipe of the equipment is a single state, so this type of equipment, namely the economizer and superheater, can use a unified model. To simplify the model, this paper makes the following assumptions [22]: (1) The energy exchange between the exhaust gas and the external environment is ignored. (2) Flow resistance is neglected. (3) The exhaust gas is in the ideal state. (4) The radiation heat is zero. (5) The intensity of the radial heat transfer is assumed to be even. (6) Radial temperature difference of pipe wall is not considered. (7) The fluid in tube is even and uncirculated. Based on energy, mass and momentum balance, the heat transfer equation among the single-phase fluid, the metal tube, and the exhaust gas can be derived as follows:

Energy balance equation of the exhaust gas is

$$\rho_g C_g V_g \frac{dT_{t,2}}{dt} = \phi_2 D_{mc} C_{\mathrm{g}} \left(T_{t,1} - T_{t,2}\right) - Q_1 \tag{19}$$

Heat exchange equation between the exhaust gas and the metal wall is

$$Q_1 = K_{y1} D_{mc} A_h \left(\left(T_{t,1} + T_{t,2}\right)/2 - T_{\mathrm{m}}\right) \tag{20}$$

Mass balance equation of the fluid is

$$D_1 - D_2 = 0 \tag{21}$$

Energy balance equation of the fluid is

$$V\rho_2 C_{p2} \frac{dT_2}{dt} = Q_2 + D_1 h_1 - D_2 h_2 \tag{22}$$

Heat exchange equation between the fluid and the metal wall is

$$Q_2 = K_{y2} D_2 A_h \left(T_m - \left(T_1 + T_2\right)/2\right) \tag{23}$$

Heat storage equation of the metal wall is

$$Q_1 - Q_2 = M_m C_m \frac{dT_m}{dt} \tag{24}$$

Where ρ_g and C_g are the density and the specific heat of the exhaust gas, ϕ_2 is the heat retention coefficient, Q_1 represents heat transfer between the exhaust gas and the metal wall, A_h is the area of heat transfer, T_m represents the temperature of the metal wall, D_2 is outlet flow of the fluid, V is the volume of heat exchanger, C_{p2} is the outlet specific heat of the fluid, Q_2 is heat transfer between the fluid and the metal wall, h_1 and h_2 represent the enthalpy of inlet and outlet fluid, K_{y1} and K_{y2} are heat transfer coefficients, M_m and C_m are the mass and the specific heat of metal.

2) Two-phase region

The two-phase region is mainly divided into the steam pack, riser tube, and downpipe, which are modelled respectively.

a. Steam drum

The modelling of the steam drum focuses on the change of the pressure and temperature of saturated vapour related to the pressure in the previous studies. The focus in this paper is the emission of the steam, so the following assumptions are made: (1) The pressure in the steam drum is considered to be uniform. (2) Steam and water are all single-phase fluid and are analysed separately in the equilibrium state. (3) The heat transfer between fluid and wall of the steam drum is ignored. (4) The density of two-phase water is calculated as the saturated water. (5) The wall temperature of the steam drum is the arithmetic mean of its internal and external temperature. (6) The pressure inside the drum does not change during normal operation [23].

The mass balance equation of steam and water is

$$\left(D_{fj}\right)_{qb} = D_{sm} + D_{ssl}\left(1 - X_{ssl}\right) - D_{pw} - D_{xje} + D_n \tag{25}$$

$$D_{ssl} X_{ssl} - D_{qb} - D_n + \left(D_{fj}\right)_{qb} = 0 \tag{26}$$

Energy balance equation is

$$D_{qb} H'' = D_{sm} H_{sm} + D_{ssl} H_{ssl} - D_{xje} H_{xje} - D_{pw} H' \tag{27}$$

Where D_{sm} and H_{sm} are outlet flow and the enthalpy of the economizer, X_{ssl} is the proportion of steam in outlet flow of riser tube, D_{ssl} and H_{ssl} are outlet flow and the enthalpy of the riser tube, D_{pw} is the flow of continuous blowdown, D_{xje} and H_{xje} are inlet flow and the enthalpy of the downpipe, D_n is the saturated steam that is condensed into water of economizer, $(D_{fj})_{qb}$ is the additional amount of steam when the pressure in the steam drum drops, D_{qb} is the outlet saturated steam of the steam drum, H' and H'' are enthalpies of the saturated water and steam.

b. Riser tube

The riser tube is where the water is heated to a mixture of water and steam. Hence, the paper makes the following simplifications [24]: (1) The resistance of the downpipe defaults to concentrate on the exit. (2) The mixture of water and steam is assumed to be a new single-phase fluid. (3) The gravity difference is not considered. (4) The inlet and outlet fluids of the riser tube are assumed to have the same parameters.

Energy, mass, and momentum balance equations of riser tube are

$$V_{ss} \frac{d\rho_{ssl}}{d\tau} = D_{xjl} - D_{ssl} \tag{28}$$

$$\rho_{ssl} V_{ss} \frac{dH_{ssl}}{d\tau} - V_{ss} \frac{dp_{ssl}}{d\tau} = D_{xjl} H_{xjl} + Q_{ss} - D_{ssl} H_{ssl} \tag{29}$$

$$L_{ss} \frac{dD_{ss}}{d\tau} = D_{xjl}^2 / \rho_{xjl} A_n - D_{ssl}^2 / \rho_{ssl} A_n \tag{30}$$

$$D_{ssev} = \left(Q_{ss} - D_{xje}\left(H' - H_{xje}\right)\right) / \left(H'' - H'\right) \tag{31}$$

$$p_{sse} - p_{ssl} - \Delta p_{ss} = 0 \tag{32}$$

$$\Delta p_{ss} = \lambda_{ss} D_{ssl}^2 / \left(\rho_{ssl} A_n^2\right) \tag{33}$$

Where V_{ss} is the volume of riser tube, D_{xjl} is the outlet flow of downpipe, D_{ssl} is the outlet flow of downpipe, H_{xjl} represents the enthalpy of outlet water of downpipe, Q_{ss} is the heat absorption of the fluid in riser tube, L_{ss} the reduced length of riser tube, p_{sse} represents the entrance pressure of riser tube, ΔP_{ss} is the pressure loss of riser tube, A_n cross-sectional area of the tube, ρ_{xjl} is the density of outlet fluid of downpipe, ρ_{ssl} is the density of outlet fluid of riser tube, H_{xje} represents enthalpy of inlet water of downpipe, D_{ssev} is evaporated flow of riser tube, λ_{ss} represents frictional resistance coefficient of riser tube.

c. Water wall

The model of the heat transfer between the exhaust gas and the metal wall is the same as the model in the single-phase region [25]. It is important to note that there is a slight difference in the model of heat transfer between the metal wall and the fluid because the fluid in the pipe is not single-phase, as shown below

$$Q_{ss} = K_n A_{ss} \left(T_m - \left(T_{ssl} + T_{sse}\right)/2\right)^3 \tag{34}$$

Where K_n is the heat transfer coefficient between the metal and the fluid of riser tube, A_{ss} is heat transfer area of riser tube, T_m represents the metal temperature.

d. Downpipe

The following assumptions are made when modelling the downpipe: (1) The water in the downpipe is saturated and the density is not considered. (2) The difference between saturated and unsaturated water is neglected, assuming that they have been mixed [26].

The momentum equations of downpipe are

$$p_{xje} - p_{xjl} + \rho' g L_{xj} - \Delta p_{xj} = 0 \tag{35}$$

$$\Delta p_{xj} = \lambda D_{xjl}^2 / \rho' A_n^2 \tag{36}$$

Where ρ' is the density of water, p_{xje} is the import pressure of downpipe, p_{xjl} is the export pressure of downpipe, Δp_{xj} is the pressure loss of downpipe, λ represents frictional resistance coefficient of the downpipe.

E. Modelling of gas-fired boiler

The working procedure of gas fired boiler is approximately divided into two steps:

(1) Exhaust gas flow: Gas and air are mixed and sprayed into the furnace through the burner, which releases heat after burning rapidly in the furnace. The intense radiation heat transfer between the wall of the furnace and the high-temperature exhaust gas is carried out to reduce the flame temperature and prevent the furnace from being burned by the high-temperature flame. Simultaneously, the high-temperature exhaust gas flows to the horizontal flue through the top of the furnace and delivers heat to the superheater arranged in the horizontal flue. Subsequently, the exhaust gas flows to the tail flue and further transfers the remaining heat to the economizer. Finally, the exhaust gas with a certain temperature is discharged into the atmosphere after this series of processes.

(2) Steam-water flow: The water supplied by the water tank is preheated by the economizer and enters the steam drum. Then the water is introduced into lower header through downpipe and heated to the mixture of water and steam in riser tube. Finally, the mixture returns to the steam drum. The entire evaporation process forms a natural circulation.

Therefore, the modelling of the gas-fired boiler is similar to the modelling of the gas cylinder of the internal combustion engine and exhaust heat boiler. There remains no need for more detailed description here. Additionally, it is necessary to add control process to the gas-fired boiler, which changes the production status of the gas-fired boiler according to the change of the required steam load to achieve the stability and economy of the boiler. The specific process is that the system can timely adjust the volume of input gas and water based on the deviation of the outlet steam. The control is PI control, whose structure flow is shown in Fig. 7.

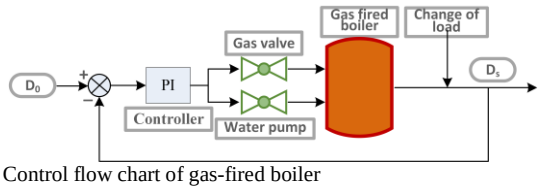

Fig. 7. Control flow chart of gas-fired boiler

F. Modelling of the synchronous generator

The model of the synchronous generator in this paper is a conventional five-order model [27].

III. Simulation Algorithm

To solve the problem of coupled systems with different time constants, a simulation algorithm is proposed, whose equation is shown in (37).

$$\begin{cases} X_1 = F_1(X_0) \\ \vdots \\ X_i = F_i\left(X_{i-1}(k_{i-1})\right), \left|X_{i-1}(k_{i-1}) - X_{i-1}(k_{i-1}-1)\right| \le \varepsilon_{i-1} \\ X_{i+1} = F_{i+1}\left(X_i(k_i)\right), \left|X_i(k_i) - X_i(k_i-1)\right| \le \varepsilon_i \\ i = 1, 2, \cdots, n \end{cases} \tag{37}$$

Where F_i is the i^{th} system, X_i is the output value of F_i, X_0 is input value of the entire system, k_i is the i^{th} step of X_i, ε_i is a minimum value of F_i, which is used to determine whether X_i is stable, n is the number of systems.

In this paper, the simulation model is divided into three parts according to the different time constants: i) the first part, which contains the gas internal combustion engine and synchronous generator, has the smallest time constant and can enter stability in around one micro-second; ii) exhaust heat exchanger and water storage tank compose the second part; iii) the third part, which includes the exhaust heat boiler and gas-fired boiler, has the biggest time constant and longest transient process. Actually, simulation contains three periods. If the results of previous period meet the requirement of the following period, for example, the electrical variables of the first part are stable, the second part will start with the output of the first part as inputs. With this method, the whole system runs smoothly.

IV. Simulations And Analysis

The system used in the simulation example serves an industrial park to meet its demand for electricity and heat. As shown in Fig. 1, there are two gas internal combustion engines, two synchronous generators with the capacity of 1.5 MW, two waste heat exchangers, two water tanks, two exhaust-heat boilers with an evaporating capacity of 0.9 t/h and three gas-fired boilers with an evaporating capacity of 4 t/h.

Based on the modelled CHP, the dynamic model of the system is constructed and simulated on MATLAB/Simulink. The key parameters are from a practical project in Shanghai, China, as shown in the Appendix. This paper mainly discusses three scenarios in Fig. 8 to verify the accuracy of the dynamic model of CHP, studies the thermoelectric interaction in the gird-connected CHP, and examines the impact of gird-connected CHP on the power grid.

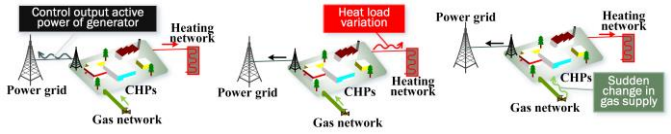

Fig. 8. Simulation scenarios

- Scenario 1 analyzes the effects of regulating the output active power of the synchronous generator on the power and heat supply parts of the grid-connected system.
- Scenario 2 analyzes the effects of changing heat load on the power and heat supply parts of the grid-connected system.
- Scenario 3 analyzes the dynamic change of the power and heat supply parts of the grid-connected system when the gas supply mutates.

A. Regulating active power output of synchronous generator

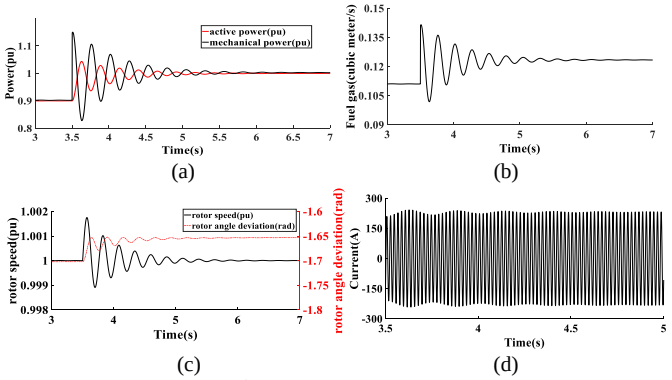

Fig. 9. Dynamic diagram of the power supply when controlling the operating mode. (a) Mechanical power and active power. (b) Fuel gas consumed by internal combustion engine. (c) Rotor speed and angle deviation. (d) Output current.

The variations of electrical variables of the synchronous generator are shown in Fig. 9 when the generator runs from 90% to being fully loaded at 3.5 s. Figure 9(a) shows the variations of active power and mechanical power of the synchronous generator. The active power increases from the original 0.9 p.u. to 1 p.u. and the input mechanical power increases. In figure 9(b), the gas of the internal combustion engine increases from 0.111 m^3/s to 0.123 m^3/s to increase the mechanical power of the synchronous generator. Figures 9(c) and 9(d) respectively depict the dynamic curves of generator speed, angle deviation and output current. It is clear that the rotor speed is stable at the rated speed and the angle deviation increases from -1.7023 rad to -1.6524 rad. The maximum output current rises from 209 A to 232 A. Fig. 9 shows that the system power supply is stable when PI controller regulates the active power of the generator.

The dynamic analysis of the heating parts of the system can be obtained from Fig. 10. In figures 10(a) and 10(b), the cooling water flow of the internal combustion engine is closely related to the air, which increases with the gas. Hence, the cooling water flow increases from 0.55 kg/s to 0.61 kg/s and the exhaust gas increases from 1.22 kg/s to 1.36 kg/s with growing air and gas. In 10(c), the input water of No. 1 water tank is the cooling water of the intercooler. When the cooling water increases at 60 s under the condition of constant water temperature, the water temperature of No. 1 water tank will subsequently increase from 30.5 ℃ to 31.2 ℃. The water of No. 1 water tank will be used as cooling water in the heat exchanger. As shown in figure 10(d), the temperature rise of cooling water in the heat exchanger at 60 s will lead to the new balance in jacket water temperature, i.e. the transition from 71 ℃ and 82 ℃ to 76 ℃ and 87 ℃. At the same time, the water temperature of No. 2 water tank is also affected, where the input and output water temperature of No. 2 water tank increase from 37.2 ℃ and 37.9 ℃ to 38.8 ℃ and 39.5 ℃.

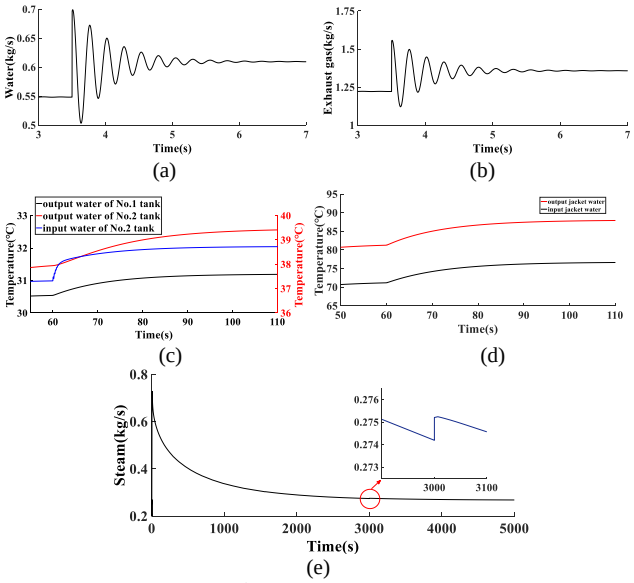

Fig. 10. Dynamic diagram of heating when controlling operating mode. (a) Input water of NO.1 water tank. (b) Exhaust gas. (c) Temperature of water storage tank. (d) Temperature of jacket water. (e) Steam flow of exhaust heat boiler.

The variations of exhaust gas flow and water temperature of No. 2 water tank will have an impact on the steam flow of exhaust heat boiler and gas-fired boiler. Figure 10(e) shows the dynamic change of the steam flow of the waste heat boiler. It can be found from the enlargement of the figure that the control of active power produces a growth effect on the steam flow at 3000 s. The impacts of the gas-fired boiler in scenario 1 and scenario 2 are both converted into the impact of the steam flow and input water temperature (No. 2 water tank) on the gas-fired boiler. Therefore, we discuss the dynamic process in scenario 2.

The assumptions at each stage of the modelling have an direct impact on the accuracy of the developed models. Although the model of each component in the CHP is independently constructed, the whole model is interconnected by the inputs and outputs of all models. Thus, the errors incurred at each modelling stage will accumulate once they are interconnected, resulting in more complicated errors. Actually, the errors can be amplified or reduced as the assumptions at each stage could positively or negatively affect the accuracy. Hence, the assessment of the overall errors cannot be simply realized by adding the errors from each step. In this paper, we record the final stable values of the inputs and outputs of critical components in simulations so that the errors incurred by all assumptions of these models are calculated respectively.

As shown in Table I, the errors between the results from the simulation and experiment of scenario 1 are very small, which demonstrate the accuracy of the developed dynamic model. When the output active power of the synchronous is adjusted from 0.9 p.u. to 1 p.u., the input fuel gas of the internal combustion changes from 0.111 m^3/s to 0.123 m^3/s in the simulation. Compared with the measured data (0.109 m^3/s and 0.121 m^3/s), the error between simulation data and experimental data is only 1.8%. Similarly, the errors of the output current of the synchronous generator, the input water flow of No. 1 water tank, the exhaust gas of the internal combustion, and the output steam flow of the exhaust heat boiler are as low as 2.4%, 3.8%, 2.3%, and 1.1% respectively.

TABLE I
DATA COMPARISON SHEET OF SCENARIO 1

SYMBOL	SIMULATION DATA	EXPERIMENTAL DATA	ERROR
D_f	0.111 to 0.123 m^3/s	0.109 to 0.121 m^3/s	1.8%
Current	209 to 232 A	204 to 227 A	2.4%
$D_{c,0}$	0.55 to 0.61 kg/s	0.53 to 0.59 kg/s	3.8%
$T_{c,1}$	30.5 to 31.2 ℃	31 to 32 ℃	2.5%
D_{mc}	1.22 to 1.36 kg/s	1.19 to 1.33 kg/s	2.3%
$T_{g,0}$	71 to 76 ℃	75 to 80 ℃	5%
$T_{g,1}$	82 to 87 ℃	86 to 91 ℃	4.6%
$T_{h,0}$	37.2 to 38.8 ℃	38.5 to 40 ℃	3.4%
$T_{h,1}$	37.9 to 39.5 ℃	39.5 to 41 ℃	4%
D_{qb}	0.274 to 0.275 kg/s	0.277 to 0.278 kg/s	1.1%

Relatively large errors appear in the simulation of the temperature of the jacket water and the water of the storage tank, which are mainly due to the variations of environment temperature.

B. Changing heat load

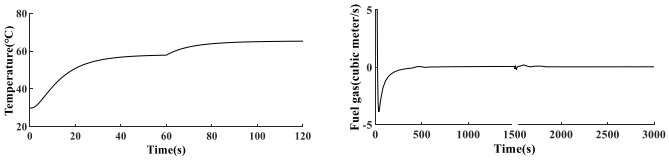

(a) (b)

Fig. 11. Dynamic diagram of the heat supply under variable heat load. (a) Water temperature of NO.2 water tank. (b) Fuel gas of gas-fired boiler

The change of heat load is realized by using the step function module on the platform of SIMULINK. The boiler is generally in operation due to the high fuel consumption of its starting procedure. When the heat load changes, it is evenly distributed via the load control model, meaning that each gas fired boiler will have the same capacity. Hence, the simulation results of a single boiler are only presented. The feed water and gas flow of the gas-fired boiler are affected by the change of heat load. The variation of feed water flow that comes from the No. 2 water tank subsequently leads to the change of the water temperature of No. 2 water tank, which has an impact on the exhaust heat boiler and fired the gas boiler.

TABLE II
DATA COMPARISON SHEET OF SCENARIO 2

SYMBOL	SIMULATION DATA	EXPERIMENTAL DATA	ERROR
$T_{h,1}$	58 to 65 ℃	56 to 63 ℃	3.2%
Fuel of GFB	0.074 to 0.044 kg/s	0.073 to 0.043 kg/s	2.3%

In 11(a), the decrease of heat load at 60 s leads to a drop in output water flow of No. 2 water tank, i.e. water flow reduces from 1.1 kg/s to 0.6 kg/s. Consequently, the temperature of No. 2 water tank increases from 58 ℃ to 65 ℃.

The variation of the steam load and water temperature of No. 2 tank will lead to the change of gas required by the boiler, as shown in figure 11(b). When steam load decreases at 1500 s, the corresponding amount of gas drops from 0.074 kg/s to 0.044 kg/s.

Additionally, the variation of steam flow of the exhaust heat boiler results in the change of the water temperature of No. 2 tank, which is consistent with the operation of the exhaust heat boiler under the scenario 1, as shown in 10(e). So, we do not repeat it here.

Table II shows small errors between the results from the simulation and experiment when the heat load is changed. Here, ignoring the invariant power supply and the exhaust heat boiler studied in scenario 1, two variables are compared. The errors of the water temperature of No. 2 water tank and the fuel gas of the gas-fired boiler are 3.2% and 2.3% respectively.

C. Changing gas supply suddenly

In the actual operation, the failure of the valve in the gas pipe failures will lead to the mutation of gas supply. Assuming a surge in gas supply, the surge would cause a rapid increase in mechanical power of the synchronous generator, affecting power supply stability. Meanwhile, if the gas-fired boiler cannot regulate the gas supply via the PI controller, the steam flow will not be sufficient for generating required heat.

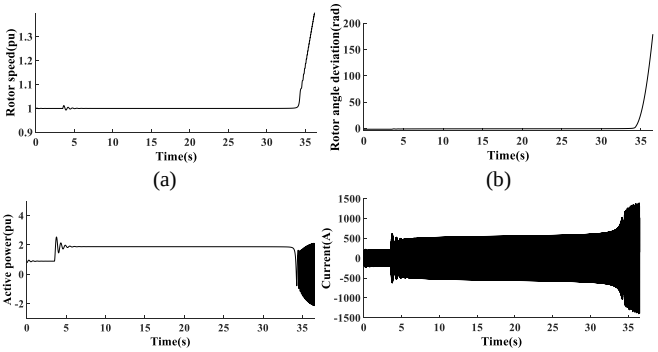

(a) (b) (c) (d)

Fig. 12. Dynamic diagram of the power supply during the internal combustion engine gas supply failure. (a) Rotor speed. (b) Rotor angle deviation. (c) Active power. (d) Output current.

In Fig. 12, if the valve fails at 3.5 s, causing the gas supply to increase from 0.111 m^3/s to 0.234 m^3/s, the synchronous generator will lose its stability. As shown, the rotation speed, rotor angle deviation, output active power and current are all out of the stable condition at around 34 s, which must be prohibited. However, the failure of the valve only makes the gas supply fixed in 0.234 m^3/s, which only produces the condition of heating similar to scenario 1, shown in Fig. 6, 7 and 8. Hence, the heating part is stable. Through the simulation analysis, it can be found that the limit value of gas supply is 0.2319 m^3/s, which can be defined as the gas supply threshold. It should be attached great importance in case that the

instability of power supply affects system security.

If the gas supply of the gas-fired boiler also fails, an increase of steam flow of gas fired boiler can be found, affecting the heating. As shown in Fig. 13, there is an obvious increase in 3000 s. At this moment, the power supply is not affected.

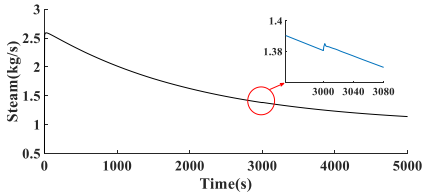

Fig. 13. Dynamic diagram of the heat supply during the internal combustion engine gas supply failure

Besides, the failure of the gas valve not only increases the gas supply but also makes the gas fall sharply. In the power supply part, the synchronous generator could reverse and consume active power from the power grid, which is contrary to the objective of CHP and thus needs to be strictly banned. In Fig. 14, if the gas supply falls to 0 kg/s, the output power of the generator and the angle difference between motor voltage and network voltage is negative, indicating the CHP absorbs power from the grid.

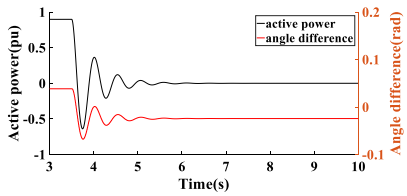

Fig. 14. Dynamic diagram of power supply during the internal combustion engine gas supply decrease

V. Conclusion

This paper proposes the time domain modelling and dynamic analysis of combined heat and power (CHP) connected to the power system. It is realized by combining existing data to analytically establish the models of the heating system. The reciprocal impact of the power supply and heating systems is analysed in 3 scenarios on the platform of MATLAB. Simultaneously, the impact of the dynamic process in CHP on the regionally integrated energy system is studied.

The dynamic model of the grid-connected CHP can accurately simulate the practical operation. And the impact of the control strategy on the system performance differs from that of another. When the control strategy is regulating the output active power of the synchronous generation by PI controller, components of the power supply part have explicit dynamic change, and components of heat supply are slightly affected, i.e., the temperature of water tanks and the steam flow of boilers rise a bit. Whereas, the control strategy that regulates heat power by the gas-fired boiler has no impact on the components of power supply part. Moreover, there exists an upper threshold value and a lower threshold value of the fuel gas consumed by the internal combustion based on its interactions with the power grid. However, the fuel gas consumed by the gas-fired boiler is not subject to this range.

Energy coupling not only increases the relationship between energy but also improves the flexibility of the energy utilization in CHP. The highly coupled energy has higher requirements on the dynamic analysis of the system in a wider region with the development of energy technology and hybrid energy network.

The work in this paper can provide a theoretical basis for modelling, joint scheduling, management and development of various energies. Future work will aim at a broader hybrid energy interconnected system, focusing on the dynamic process and stability control of large systems and the dynamic modelling and operation of energy internet.

References

[1] Chen X, Kang C, O'Malley M, et al. Increasing the flexibility of combined heat and power for wind power integration in China: Modelling and implications[J]. IEEE Transactions on Power Systems, 2015, 30(4): 1848-1857.

[2] Smith A D，Mago P J，Fumo N. Benefits of thermal energy storage option combined with CHP system for different commercial building types[J]. Sustainable Energy Technologies & Assessment，2013，1：3-12.

[3] Sun Z， Li L，Bego A，et al. Customer-side electricity load management for sustainable manufacturing systems utilizing combined heat and power generation system[J] . International Journal of Production Economics，2015，165：112-119.

[4] Hashemi R. A developed offline model for optimal operation of combined heating and cooling and power systems[J]. IEEE Transactions on Energy Conversion, 2009, 24(1): 222-229.

[5] Xie D, Lu Y, Sun J, et al. Optimal Operation of a Combined Heat and Power System Considering Real-time Energy Prices[J]. IEEE Access, 2016, 4: 3005-3015.

[6] Wang J，Zhai Z，Jing Y，et al. Optimization design of BCHP system to maximize to save energy and reduce environmental impact[J]. Energy，2010，35(8)：3388-3398.

[7] Kavvadias K C，Maroulis Z B. Multi-objective optimization of a trigeneration plant[J]. Energy Policy，2010，38(2)：945-954.

[8] Hellmers A, Zugno M, Skajaa A, et al. Operational strategies for a portfolio of wind farms and CHP plants in a two-price balancing market[J]. IEEE Transactions on Power Systems, 2016, 31(3): 2182-2191.

[9] Wang Y, Bermukhambetova A, Wang J H, et al. Modelling of the Whole Process of a University Campus CHP Power Plant and Dynamic Performance Study[J]. International Journal of Automation and Computing, 2016, 13(1):53-63.

[10] Tatarinova N V, Suvorov D M. Development of adequate computational mathematical models of cogeneration steam turbines for solving problems of optimization of operating modes of CHP plants[C]// International Conference on Industrial Engineering, Applications and Manufacturing. IEEE, 2017:1-6.

[11] Pirouti M, Wu J, Ekanayake J, et al. Dynamic modelling and control of a direct-combustion biomass CHP unit[C]// Universities Power Engineering Conference. 2010:1-6.

[12] Liu N, Yu X, Wang C, et al. Energy-Sharing Model With Price-Based Demand Response for Microgrids of Peer-to-Peer Prosumers[J]. IEEE Transactions on Power Systems, 2017, 32(5):3569-3583.

[13] Abunku M, Melis W J C. Modelling of a CHP system with electrical and thermal storage[C]//Power Engineering Conference (UPEC), 2015 50th International Universities. IEEE, 2015: 1-5.

[14] Wang Y, Bermukhambetova A, Wang J, et al. Dynamic modelling and simulation study of a university campus CHP power plant[C]//Automation and Computing (ICAC), 2014 20th International Conference on. IEEE, 2014: 3-8.

[15] Dai Y, Chen L, Min Y, et al. Dispatch model of combined heat and power plant considering heat transfer process[J]. IEEE Transactions on Sustainable Energy, 2017.

[16] Massucco S, Pitto A, Silvestro F. A Gas Turbine Model for Studies on Distributed Generation Penetration Into Distribution Networks[J]. IEEE Transactions on Power Systems, 2011, 26(3):992-999.

[17] Jia N, Wang J, Nuttall K, et al. HCCI engine modelling for real-time 8implementation and control development[J]. IEEE/ASME Transactions on Mechatronics, 2007, 12(6): 581-589.
[18] Kolmanovsky I, Morall P, Van Nieuwstadt M, et al. Issues in modelling and control of intake flow in variable geometry turbocharged engines[J]. Chapman and Hall CRC research notes in mathematics, 1999: 436-445.
[19] Hendricks E, Sorenson S C. Mean value modelling of spark ignition engines[R]. SAE Technical paper, 1990.
[20] Gao T, Sammakia B G, Murray B T, et al. Cross flow heat exchanger modelling of transient temperature input conditions[J]. IEEE Transactions on Components, Packaging and Manufacturing Technology, 2014, 4(11): 1796-1807.
[21] Nash A L, Badithela A, Jain N. Dynamic modelling of a sensible thermal energy storage tank with an immersed coil heat exchanger under three operation modes[J]. Applied Energy, 2017, 195: 877-889.
[22] Ashok S, Banerjee R. Optimal operation of industrial cogeneration for load management[J]. IEEE Transactions on power systems, 2003, 18(2): 931-937.
[23] Takaghaj S M, Macnab C J B, Westwick D, et al. Neural-adaptive control of waste-to-energy steam generators[J]. IEEE Transactions on Control Systems Technology, 2014, 22(5): 1920-1926.
[24] ALOBAID F，STROHLE J，EPPLE B，et al．Dynamic simulation of a supercritical once-through heat recovery steam generator during load changes and start-up procedures[J]．Hydrotechnical Construction，2009，86(7/8)：1274-1282．
[25] Kakimoto N, Baba K. Performance of gas turbine-based plants during frequency drops[J]. IEEE Transactions on Power systems, 2003, 18(3): 1110-1115.
[26] Molina D L, Vidal J R, Gonzalez F. Mathematical Modelling Based on Exergy Analysis for a Bagasse Boiler[J]. IEEE Latin America Transactions, 2017, 15(1): 65-74.
[27] Hammons T J, Winning D J. Comparisons of synchronous-machine models in the study of the transient behavior of electrical power systems[J]. Proceedings of the Institution of Electrical Engineers. IET Digital Library, 1971, 118(10): 1442-1458.

Appendix

TABLE I
SIMULATION PARAMETERS

TURBINE COMPRESSOR		INTERCOOLER	
Symbol	VALUE	Symbol	VALUE
k	1.3	ϕ_1	0.84
π_c	12	Δp_{it}^0	400 pa
η_c	0.98	D_{a0}	3 kg/s
R	287 J/(kg·K)	K_1	0.65
η_t	0.6	K_2	0.185
π_t	4	K_3	0.463
η_{tc}	0.95		
I_{tc}	$2.5\cdot10^{-3}$ kg·m^2		
GAS CYLINDER		Exhaust heat exchanger	
Symbol	VALUE	symbol	value
H_u	40.63 MJ/m^3	C_{p1}	3165 J/(kg·K)
η_m	0.9	C_{p2}	4179 J/(kg·K)
ς_w	0.05	K_{e1}	66.5 w/(m^2·K)
C_w	4.2 kJ/(kg·K)	K_{e2}	279.7 w/(m^2·K)
C_{pa}	127 J/(kg·K)	A_1	11.6 m^3
C_{pg}	127 kJ/(kg·K)	A_2	3.2 m^3
		m	25 kg
		C_h	502.4 J/(kg·K)
Water tank		PI controller	
symbol	value	symbol	value
M_0	50 kg	Synchronous generator	
λ_c	0.75	K_{i1}	0.1
h_c	3.5 m	K_{p1}	0.4
d_{c1}	1.6 m	Gas fired boiler	
d_{c2}	2 m	K_{i2}	-0.08
δ_c	0.2 m	K_{p2}	-5.09
Exhaust heat boiler			
symbol	value	symbol	value
ρ_g	1.2118 kg/m^3	K_{y2}	42.2 w/(m^2·℃)
C_g	1.03 KJ/(kg·K)	A_h	150 m^2
V_g	15.6 m^3	V	3.12 m^3
ϕ_2	0.85	C_{p2}	4.2 kJ/(kg·K)
K_{y1}	45.6 w/(m^2·℃)	M_m	30 kg
C_m	502.4 J/(kg·K)	H''	2748 KJ/kg
V_{ss}	1.9 m^3	λ	0.025
L_{ss}	40 m	ρ'	916 kg/m^3
A_n	$1.6*10^{-3}$ m^2	K_n	42.2 w/(m^2·℃)
λ_{ss}	0.025	A_{ss}	150 m^2
H'	640 KJ/kg		